AERIAL BASE STATION PLACEMENT LEVERAGING RADIO TOMOGRAPHIC MAPS

Daniel Romero[1]*, Pham Q. Viet*[1]*, and Geert Leus*[2]

[1] University of Agder, Norway. Email {daniel.romero,viet.q.pham}@uia.no
[2] Delft University of Technology, The Netherlands. Email: g.j.t.1eus@tudelft.nl

ABSTRACT

Mobile base stations on board unmanned aerial vehicles (UAVs) promise to deliver connectivity to those areas where the terrestrial infrastructure is overloaded, damaged, or absent. A fundamental problem in this context involves determining a minimal set of locations in 3D space where such aerial base stations (ABSs) must be deployed to provide coverage to a set of users. While nearly all existing approaches rely on average characterizations of the propagation medium, this work develops a scheme where the actual channel information is exploited by means of a radio tomographic map. A convex optimization approach is presented to minimize the number of required ABSs while ensuring that the UAVs do not enter no-fly regions. A simulation study reveals that the proposed algorithm markedly outperforms its competitors.

***Index Terms*—** Aerial base stations, radio tomography, radio maps, spectrum cartography, placement.

1. INTRODUCTION

The rapid evolution of unmanned aerial vehicles (UAVs) has spurred extensive research to complement terrestrial communication infrastructure with base stations mounted on board them [1]. The main use case of such *aerial base stations* (ABSs) is to provide connectivity in areas where it is insufficient or not available, e.g. because they are remote or because of a natural disaster. The research question that arises is at which locations one or multiple ABSs need to be deployed to provide coverage to the ground terminals (GTs).

This question has been extensively investigated for a single ABS; see e.g. [2–5]. Other schemes have been proposed to set the 2D position of multiple ABSs in a horizontal plane of a given height; see e.g. [6]. In contrast, the focus here is on algorithms capable of determining the 3D position of the ABSs. Existing works in this context are classified next according to how they account for the propagation channel between the ABSs and the GTs. First, some schemes [7] do not model or learn the channel and, therefore, the suitability of a location cannot be determined before an ABS visits it, which drastically increases the time to find a suitable placement. Besides approaches that assume free-space propagation [8], a large number of works rely on the empirical model from [9]; see e.g. [10–14].The main limitation is that such models provide shadowing values in *average scenarios*, e.g. in a generic urban environment, but are likely to yield highly suboptimal placements in a specific environment. This limitation is addressed in [15, 16] by using 3D models of the deployment scenario. Unfortunately, 3D models are seldom available and, even when they are, their resolution is insufficient for reasonably predicting the channel in conventional bands or, for example, when a GT is inside a building.

This work was supported by the Research Council of Norway through the IKTPLUSS Grant 311994.

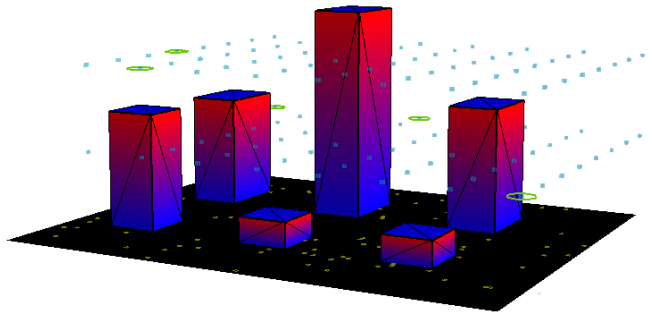

Fig. 1: Example of ABS placement in an urban environment with the developed simulator. GTs are represented by markers on the ground, grid points by blue dots, and ABS positions by green circles.

In contrast, the present paper proposes a scheme where the air-to-ground channel of the *specific* deployment scenario is learned by relying on the notion of *radio tomography* [17,18]. A *radio map* that provides the attenuation between arbitrary points of space is constructed based on measurements collected by the GTs and ABSs. To accommodate the special requirements of air-to-ground radio maps, the conventional approach to radio tomography, which has a cubic complexity in the size of the grid, is here replaced with a linear complexity algorithm. Using this radio map, a placement algorithm is proposed to minimize the number of ABSs required to guarantee a minimum rate for all GTs. Unlike most competing algorithms, it is based on a convex program, it can accommodate no-fly zones, and has low computational complexity. The third contribution is an open source simulator[1] that allows testing and developing algorithms for ABS placement; see Fig. 1.

Paper structure. Sec. 2 and formulates the problem. The construction and evaluation of radio maps is described in Sec. 3. An algorithm for ABS placement using radio maps is then proposed in Sec. 4. Performance evaluation is carried out in Sec. 5 by means of the developed simulator. Finally, Secs. 6 and 7 respectively discuss the related work and present the main conclusions. The supplementary material [19] contains an algorithm for approximating tomographic integrals and the derivation of the placement algorithm.

Notation. $\mathbb{R}_+$ is set of non-negative real numbers. Boldface uppercase (lowercase) letters denote matrices (column vectors). $a[i]$ represents the i-th entry of vector $\boldsymbol{a}$. Notation $\mathbf{0}$ (respectively $\mathbf{1}$) refers to the matrix of the appropriate dimensions with all zeros (ones). $\|\boldsymbol{A}\|_{\mathrm{F}}$ denotes Frobenius norm of matrix $\boldsymbol{A}$, whereas $\|\boldsymbol{a}\|_p$ denotes the ℓ_p-norm of vector $\boldsymbol{a}$. With no subscript, $\|\boldsymbol{a}\|$ stands for the ℓ_2-norm. Inequalities between vectors or matrices must be understood entrywise.

[1] https://github.com/uiano/abs_placement_via_radio_maps

2. MODEL AND PROBLEM FORMULATION

Consider M users or ground terminals (GTs) located at positions $\{\boldsymbol{x}_1^{\text{GT}}, \ldots, \boldsymbol{x}_M^{\text{GT}}\} \subset \mathcal{X} \subset \mathbb{R}^3$, where region $\mathcal{X}$ will typically include points on the ground and inside buildings. To provide connectivity to the GTs, N ABSs are deployed at positions $\{\boldsymbol{x}_1^{\text{ABS}}, \ldots, \boldsymbol{x}_N^{\text{ABS}}\} \subset \mathcal{F} \subset \mathbb{R}^3$, where $\mathcal{F}$ comprises all locations where a UAV is allowed to fly. This excludes no-fly zones, airspace occupied by buildings, and altitudes out of legal limits. To simplify the exposition, the focus will be on the downlink and it will be assumed that the channel is not frequency dispersive. The rate of the communication link between the m-th GT and an ABS at position $\boldsymbol{x}^{\text{ABS}} \in \mathcal{X}$ is determined by the channel gain and noise power. The former is given by

$$\gamma_m(\boldsymbol{x}^{\text{ABS}}) = 20\log_{10}\left(\frac{\lambda}{4\pi\|\boldsymbol{x}_m^{\text{GT}} - \boldsymbol{x}^{\text{ABS}}\|}\right) - \xi(\boldsymbol{x}_m^{\text{GT}}, \boldsymbol{x}^{\text{ABS}}), \quad (1)$$

where λ is the wavelength associated with the carrier frequency of the transmission and function ξ denotes shadowing. Small-scale fading is ignored for simplicity, but the ensuing formulation can be adapted to accommodate the associated uncertainty. The capacity is

$$C_m(\boldsymbol{x}^{\text{ABS}}) = W\log_2\left(1 + P_{\text{TX}}10^{\gamma_m(\boldsymbol{x}^{\text{ABS}})/10}/\sigma^2\right), \quad (2)$$

where W denotes bandwidth, P_{TX} the transmit power, and σ^2 the noise power. Since the m-th GT may connect to one or multiple ABSs, it may receive a rate up to $\sum_n C_m(\boldsymbol{x}_n^{\text{ABS}})$. As usual in the literature, it is assumed that the backhaul connection of the ABSs has sufficiently high capacity, yet the proposed scheme can be generalized to accommodate backhaul constraints.

The problem is to find a minimal set of ABS locations that guarantees a minimum rate for every user. This criterion arises naturally in some of the main use cases of UAV-assisted networks such as emergency response or disaster management. Formally, the problem can be stated as follows:

$$\underset{N, \{\boldsymbol{x}_n^{\text{ABS}}\}_{n=1}^N}{\text{minimize}} \quad N \quad (3a)$$

$$\text{s.t.} \ \sum_n C_m(\boldsymbol{x}_n^{\text{ABS}}) \geq r_{\min}, \ m = 1, \ldots, M, \quad (3b)$$

$$\boldsymbol{x}_n^{\text{ABS}} \in \mathcal{F}, \ n = 1, \ldots, N. \quad (3c)$$

To simplify notation, the same rate $r_{\min}$ is assumed across GTs, but different rates can be set up to straightforward modifications.

3. TOMOGRAPHIC RADIO MAPS

The first difficulty when solving (3) is that the function $C_m(\boldsymbol{x}^{\text{ABS}})$ is unknown since the shadowing term $\xi(\boldsymbol{x}_m^{\text{GT}}, \boldsymbol{x}^{\text{ABS}})$ in (1) is unknown. The approach proposed here is to rely on a radio map that provides $\xi(\boldsymbol{x}^{\text{GT}}, \boldsymbol{x}^{\text{ABS}})$ for all $\boldsymbol{x}^{\text{GT}}$ and $\boldsymbol{x}^{\text{ABS}}$. Such a map can be constructed by means of the so-called tomographic (or NeSh) model [17], as considered in the literature of channel-gain cartography; see [20] and references therein. However, the existing works in this context focus on ground-to-ground channels. Constructing radio maps of air-to-ground channels involves special challenges that render existing approaches unsuitable, as discussed later.

The radio tomographic model [17] prescribes that

$$\xi(\boldsymbol{x}_1, \boldsymbol{x}_2) = \frac{1}{\|\boldsymbol{x}_1 - \boldsymbol{x}_2\|_2^{1/2}} \int_{\boldsymbol{x}_1}^{\boldsymbol{x}_2} l(\boldsymbol{x}) d\boldsymbol{x}, \quad (4)$$

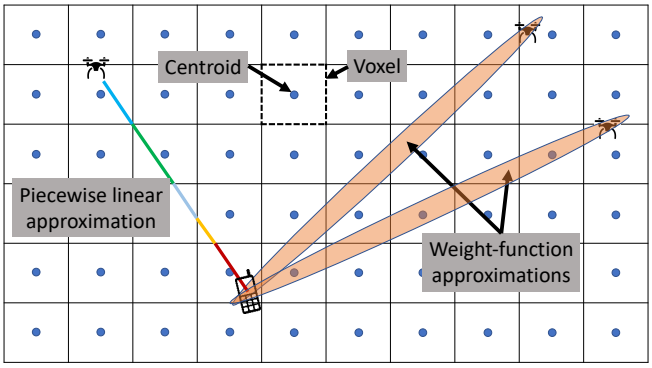

Fig. 2: 2D illustration of the conventional weight-function approximation of the tomographic integral (4) (orange ellipses) and the approximation adopted here (colored line segment). Observe that the upper ellipse contains no centroid and, therefore, the approximation will yield zero attenuation regardless of the values of the SLF.

where the function l inside the line integral is termed *spatial loss field* (SLF) and quantifies the local attenuation (absorption) that a signal suffers at each position. The SLF can be estimated in a first stage before solving (3) by collecting measurements of the form $(\boldsymbol{x}^{\text{ABS}}, \boldsymbol{x}^{\text{GT}}, \gamma_m(\boldsymbol{x}^{\text{ABS}}))$ and applying standard estimation techniques; see e.g. [20–22].

In practice, to estimate l and evaluate (4), function l needs to be discretized by storing its values $l(\boldsymbol{x}_1^{\bar{\mathcal{X}}}), \ldots, l(\boldsymbol{x}_Q^{\bar{\mathcal{X}}})$ on a 3D regular grid of Q points $\bar{\mathcal{X}} := \{\boldsymbol{x}_1^{\bar{\mathcal{X}}}, \ldots, \boldsymbol{x}_Q^{\bar{\mathcal{X}}}\}$. The conventional approach approximates (4) as a weighted sum [23] of the values $l(\boldsymbol{x}_q^{\bar{\mathcal{X}}})$ for which the centroid $\boldsymbol{x}_q^{\bar{\mathcal{X}}}$ lies inside an ellipsoid with foci at $\boldsymbol{x}_1$ and $\boldsymbol{x}_2$; see the ellipses in Fig. 2 for a depiction in 2D. Unfortunately, it can be easily seen from Fig. 2 that the resulting approximation of $\xi(\boldsymbol{x}_1, \boldsymbol{x}_2)$ is a discontinuous function of $\boldsymbol{x}_1$ and $\boldsymbol{x}_2$. It may even be 0 even when $l(\boldsymbol{x}_q^{\bar{\mathcal{X}}}) \neq 0 \ \forall q$. To minimize these effects, the grid point spacing needs to be small relative to the length of the minor axis, which is commonly set in the order of the wavelength. Thus, for standard centimetric wavelengths and regions $\mathcal{X}$ with sides in the order of km and height in the order of 100 m, Q must be in the order of 10^{14}, which is prohibitively high. Finally, the complexity of such an approximation is $\mathcal{O}(Q_0^3)$ for a $Q_0 \times Q_0 \times Q_0$ grid.

To remedy these issues, this paper advocates approximating the integral in (4) as a line integral of a piecewise constant approximation of l, as already hinted in [22] for tomographic imaging. This involves obtaining the intersections between the the voxel boundaries and the line segment that connects the transmitter to the receiver locations; see the colored segment in Fig. 2. A possible implementation along the lines of [24, Sec. I-B-1] is presented in the supplementary material [19], but others are possible. The resulting approximation is continuous, can be used with large grid point spacing, and can be computed with complexity only $\mathcal{O}(Q_0)$ for a $Q_0 \times Q_0 \times Q_0$ grid.

4. PLACEMENT WITH MIN-RATE GUARANTEES

The approach in Sec. 3 makes it possible to find the shadowing between any two points and, therefore, the channel gain and capacity; cf. (1) and (2). The constraint in (3b) can thus be evaluated. Yet, solving (3) is challenging: even if N were known and one just needed to find feasible $\{\boldsymbol{x}_n^{\text{ABS}}\}_{n=1}^N$, the problem would still be non-

convex due to the constraints. To bypass this difficulty, the proposed approach involves discretizing the flight region $\mathcal{F}$ into a *flight grid* $\bar{\mathcal{F}} := \{\boldsymbol{x}_1^{\bar{\mathcal{F}}}, \ldots, \boldsymbol{x}_G^{\bar{\mathcal{F}}}\} \subset \mathcal{F} \subset \mathbb{R}^3$; see Fig. 1.

Since $\bar{\mathcal{F}}$ contains only points where an ABS can be placed, solving (3) amounts to finding the smallest subset of N points of $\bar{\mathcal{F}}$ that satisfies (3b). To see this, replace $\boldsymbol{x}_n^{\text{ABS}} \in \mathcal{F}$ in (3c) with $\boldsymbol{x}_n^{\text{ABS}} \in \bar{\mathcal{F}}$ and let α_g be 1 if there is an ABE at $\boldsymbol{x}_g^{\bar{\mathcal{F}}}$ and 0 otherwise. The summation in (3b) can then be expressed as $\sum_g \alpha_g C_m(\boldsymbol{x}_g^{\bar{\mathcal{F}}})$. Since the number of ABSs can be written as $\sum_g \alpha_g$, the discretized version of (3) becomes

$$\underset{\boldsymbol{\alpha}\in\{0,1\}^G}{\text{minimize}} \quad \textstyle\sum_g \alpha_g \tag{5a}$$

$$\text{s.t.} \quad \textstyle\sum_g \alpha_g \boldsymbol{c}_g \geq r_{\text{min}}\mathbf{1}, \tag{5b}$$

where $\boldsymbol{c}_g := [C_1(\boldsymbol{x}_g^{\bar{\mathcal{F}}}), \ldots, C_M(\boldsymbol{x}_g^{\bar{\mathcal{F}}})]^\top$. Problem (5) is of a combinatorial nature and can be solved for small G by exhaustive search. However, the complexity of such a task is exponential and, therefore, it is preferable to adopt an approximation that can be efficiently computed. One possibility is to relax the constraint $\boldsymbol{\alpha} \in \{0,1\}^G$ as well as the objective and apply an interior-point solver. This approach is described in the supplementary material [19] but not pursued here due to the well-known poor scalability of this kind of methods with the number of variables and constraints [25]. Indeed, in this application, G can be in the order of millions, which would render the cubic complexity of interior-point methods prohibitive. Instead, this section presents a solver based on the *alternating-direction method of multipliers* (ADMM) [26] whose complexity is linear in G.

Suppose that there exists no grid point such that $\boldsymbol{c}_g = \mathbf{0}$. Otherwise, $\boldsymbol{x}_g^{\bar{\mathcal{F}}}$ can be disregarded without further implications. By applying the change of variables $\alpha_g \boldsymbol{c}_g \to \boldsymbol{r}_g$, it is clear that Problem (5) can be equivalently written as

$$\underset{\boldsymbol{R}\in\mathbb{R}^{M\times G}}{\text{minimize}} \quad \textstyle\sum_{g=1}^G \mathbb{I}[\boldsymbol{r}_g \neq \mathbf{0}] \tag{6a}$$

$$\text{s.t.} \quad \textstyle\sum_{g=1}^G \boldsymbol{r}_g \geq r_{\text{min}}\mathbf{1} \tag{6b}$$

$$\boldsymbol{r}_g \in \{\mathbf{0}, \boldsymbol{c}_g\},\ g = 1, \ldots, G, \tag{6c}$$

where $\boldsymbol{R} := [\boldsymbol{r}_1, \ldots, \boldsymbol{r}_G]$ and $\mathbb{I}[\cdot]$ is a function that returns 1 when the condition in brackets holds and 0 otherwise. It will now be argued that relaxing the constraint $\boldsymbol{r}_g \in \{\mathbf{0}, \boldsymbol{c}_g\}$ as $\mathbf{0} \leq \boldsymbol{r}_g \leq \boldsymbol{c}_g$ entails no loss of optimality. On the one hand, if $\{\boldsymbol{r}_g\}_g$ are feasible for (6), then they are feasible for the relaxed problem and yield the same objective value. On the other hand, if $\{\boldsymbol{r}_g\}_g$ are feasible for the relaxed problem, setting those non-zero $\boldsymbol{r}_g$ equal to $\boldsymbol{c}_g$ yields a feasible point for (6) that attains the same objective value.

The next step is to show that, after relaxing (6c), the inequality in (6b) can be replaced with an equality without loss of optimality. First, note that (6b) can be written as $\boldsymbol{R}\mathbf{1} \geq r_{\text{min}}\mathbf{1}$. Upon letting $\bar{\boldsymbol{r}}_m \in \mathbb{R}^G$ denote the m-th column of $\boldsymbol{R}^\top$, constraint (6b) becomes $\bar{\boldsymbol{r}}_m^\top \mathbf{1} \geq r_{\text{min}},\ m = 1, \ldots, M$. Now consider a feasible $\boldsymbol{R}$ and note that if $\bar{\boldsymbol{r}}_{m_0}^\top \mathbf{1} > r_{\text{min}}$ for some m_0, then replacing $\bar{\boldsymbol{r}}_{m_0}$ with $\bar{\boldsymbol{r}}'_{m_0} := r_{\text{min}}\bar{\boldsymbol{r}}_{m_0}/(\mathbf{1}^\top \bar{\boldsymbol{r}}_{m_0})$ yields another feasible $\boldsymbol{R}'$ that satisfies $(\bar{\boldsymbol{r}}'_{m_0})^\top \mathbf{1} = r_{\text{min}}$ and that attains the same objective value as $\boldsymbol{R}$. Applying this logic for all m yields a feasible matrix that satisfies $\boldsymbol{R}\mathbf{1} = r_{\text{min}}\mathbf{1}$ without affecting the objective value.

The objective $\sum_{g=1}^G \mathbb{I}[\boldsymbol{r}_g \neq \mathbf{0}]$ can be equivalently expressed as $\sum_{g=1}^G \mathbb{I}[\|\boldsymbol{r}_g\|_\infty \neq \mathbf{0}]$, where the ℓ_∞-norm $\|\boldsymbol{v}\|_\infty$ equals the largest absolute value of the entries of vector $\boldsymbol{v}$. Clearly, $\sum_{g=1}^G \mathbb{I}[\|\boldsymbol{r}_g\|_\infty \neq \mathbf{0}] = \|[\|\boldsymbol{r}_1\|_\infty, \ldots, \|\boldsymbol{r}_G\|_\infty]^\top\|_0$, which suggests the relaxation $\|[\|\boldsymbol{r}_1\|_\infty, \ldots, \|\boldsymbol{r}_G\|_\infty]^\top\|_1 = \sum_g \|\boldsymbol{r}_g\|_\infty$, or its reweighted version $\sum_g w_g \|\boldsymbol{r}_g\|_\infty$, where $\{w_g\}_g$ are non-negative constants set as in [27]. With these observations, the problem becomes

$$\underset{\boldsymbol{R}\in\mathbb{R}^{M\times G}}{\text{minimize}} \quad \textstyle\sum_g w_g \|\boldsymbol{r}_g\|_\infty \tag{7a}$$

$$\text{s.t.} \quad \boldsymbol{R}\mathbf{1} = r_{\text{min}}\mathbf{1},\ \mathbf{0} \leq \boldsymbol{R} \leq \boldsymbol{C}, \tag{7b}$$

where the (m,g)-th entry of $\boldsymbol{C} \in \mathbb{R}_+^{M\times G}$ is given by $c_{m,g} := C_m(\boldsymbol{x}_g^{\bar{\mathcal{F}}})$, i.e., the capacity of the link between the m-th user and the g-th grid point. The (m,g)-th entry of $\boldsymbol{R}$ therefore satisfies $0 \leq r_{m,g} \leq c_{m,g}$, which means that it can be interpreted as the rate at which a *virtual ABS* placed at grid point $\boldsymbol{x}_g^{\bar{\mathcal{F}}}$ communicates with the m-th user. In case that $r_{m,g} = 0$ for all m, then no *actual* ABS needs to be deployed at $\boldsymbol{x}_g^{\bar{\mathcal{F}}}$. In other words, the virtual ABS at $\boldsymbol{x}_g^{\bar{\mathcal{F}}}$ corresponds to an actual ABS only if $r_{m,g} \neq 0$ for some m.

Within the ADMM framework, Problem (7) can be decomposed into one subproblem per row and column of $\boldsymbol{R}$. Each problem involves solving a bisection task of a 1D monotonically decreasing function and therefore can be solved with $\mathcal{O}(1)$ evaluations. The total complexity is $\mathcal{O}(MG)$, much smaller than the $\mathcal{O}((G+2M)^3)$ complexity per inner iteration of an interior-point method; cf. the supplementary material [19]. The algorithm is shown as Algorithm 1 and is derived in the supplementary material. In the notation used therein, if $\boldsymbol{A}$ is a matrix, then $\boldsymbol{a}_m$ is its m-th column and $\bar{\boldsymbol{a}}_n^\top$ its n-th row. Furthermore, superscripts indicate the iteration index, $\rho > 0$ is the step size, and the min and max operators act entrywise.

Algorithm 1: ABS Placement

Data: $\boldsymbol{C} \in \mathbb{R}_+^{M\times G}$, $r_{\text{min}} \in \mathbb{R}_+$, $\{w_g\}_g \subset \mathbb{R}_+$, $\rho > 0$
Initialize $\boldsymbol{U}^1 \in \mathbb{R}_+^{M\times G}$ and $\boldsymbol{Z}^1 \in \mathbb{R}_+^{M\times G}$
for $k = 1, 2, \ldots$ **do**
  for $g = 1, 2, \ldots, G$ **do**
    Bisection: find s_g^{k+1} s.t. $\mathbf{1}^\top \max(\boldsymbol{z}_g^k - \boldsymbol{u}_g^k - s_g^{k+1}\mathbf{1}, \mathbf{0}) = w_g/\rho$
    Set $\boldsymbol{r}_g^{k+1} = \min(\boldsymbol{z}_g^k - \boldsymbol{u}_g^k, s_g^{k+1}\mathbf{1})$
  for $m = 1, 2, \ldots, M$ **do**
    Bisection: find λ s.t. $\mathbf{1}^\top \max(\mathbf{0}, \min(\bar{\boldsymbol{c}}_m, \bar{\boldsymbol{r}}_m^{k+1} + \bar{\boldsymbol{u}}_m^k - \lambda\mathbf{1})) = r_{\text{min}}$
    Set $\bar{\boldsymbol{z}}_m^{k+1} = \max(\mathbf{0}, \min(\bar{\boldsymbol{c}}_m, \bar{\boldsymbol{r}}_m^{k+1} + \bar{\boldsymbol{u}}_m^k - \lambda\mathbf{1}))$
  Set $\boldsymbol{U}^{k+1} = \boldsymbol{U}^k + \boldsymbol{R}^{k+1} - \boldsymbol{Z}^{k+1}$
  If convergence( ) **then** return $\boldsymbol{R}^{k+1}$

5. NUMERICAL EXPERIMENTS

The area of interest is a rectangle of 500×400 m with 9 streets in each direction delimited by 8 rows and columns of buildings of a certain height h. The flight height is between 50 and 150 m. The SLF is such that the absorption inside the buildings is 3 dB/m. The carrier frequency is 2.4 GHz, the bandwidth $W = 20$ MHz, the transmit power $P_{\text{TX}} = 0.1$ Watt, and the noise power $\sigma^2 = -96$ dBm. A total of M GTs are deployed on the street uniformly at random. The proposed algorithm is compared with the algorithm by Huang et al. [28], the K-means algorithm by Galkin et al. [29], the spiral-based algorithm by Lyu et al. [30], and the iterative algorithm by Hammouti et al. [11] for unlimited backhaul. The implementation of the algorithm in [28] was provided by the authors, whereas the rest were implemented by us. The algorithm in [28] is only used in one

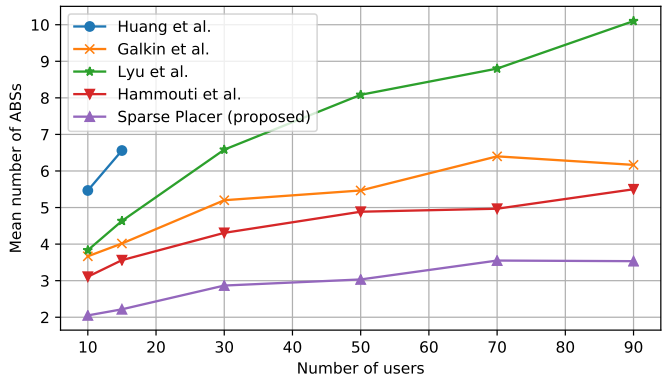

Fig. 3: Mean minimum number of ABSs required to provide a minimum rate of $r_{\min} = 5$ Mb/s vs. the number of GTs ($h = 53$ m, $20 \times 30 \times 5$ SLF grid, $9 \times 9 \times 3$ fly grid).

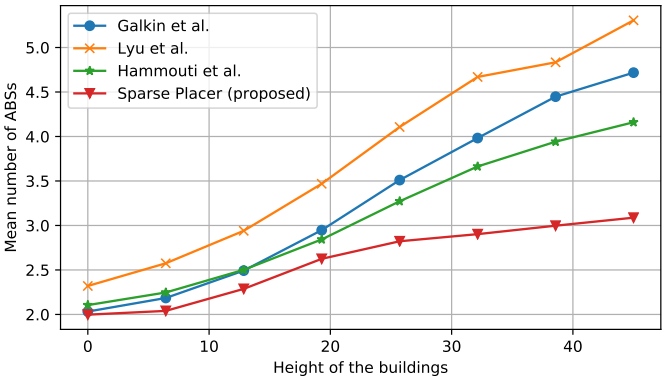

Fig. 4: Mean minimum number of ABSs required to provide a minimum rate of $r_{\min} = 20$ Mb/s vs. h [m] ($20 \times 30 \times 150$ SLF grid, $9 \times 9 \times 5$ fly grid).

experiment since its computational complexity of $\mathcal{O}(M^6)$ makes it only suitable for a relatively low M. The positions returned by these algorithms are projected onto the grid $\bar{\mathcal{F}}$ of allowed flying positions.

The adopted performance metric is the minimum number of ABSs required to guarantee a rate $r_{\min}$ to all GTs. This metric is averaged using Monte Carlo across realizations of the user locations. For the algorithms in [28] and [30], which are based on a maximum radius, the latter is gradually decreased starting from its value corresponding to free space propagation until all GTs receive the minimum rate. For the algorithms in [11] and [29], the number of centroids is gradually increased starting from 1 until the aforementioned rate condition is met. See the repository (link on the first page) for more details along with the code of all experiments.

Fig. 3 depicts the minimum number of ABSs required to guarantee a rate of $r_{\min} = 5$ Mb/s for all GTs. The proposed algorithm is seen to yield placements that require fewer ABSs than all competing algorithms. This can be ascribed to the fact that it is aware of the channel and of in which regions it is allowed to fly. To investigate further the impact of the former effect, Fig. 4 studies the influence of shadowing. For a building height $h = 0$, propagation occurs in free space, which leads to all algorithms performing similarly. The slightly worse performance of the algorithm by Lyu et al. is mainly caused by the flight grid discretization. As h increases, the channel gradually differs more and more from free-space propagation and

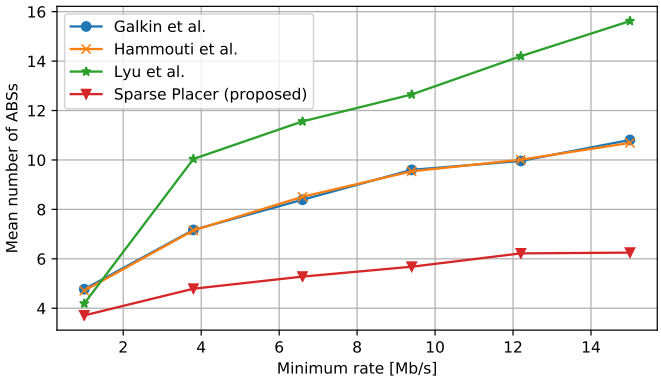

Fig. 5: Mean minimum number of ABSs required to provide a minimum rate of $r_{\min}$ ($h = 53$ m, $48 \times 40 \times 5$ SLF grid, $9 \times 9 \times 5$ fly grid).

the competing algorithms suffer a performance degradation.

Finally, Fig. 5 investigates the influence of $r_{\min}$. It is seen that the sensitivity of the proposed algorithm is much smaller than the one of its competitors, for which the performance metric increases considerably as $r_{\min}$ increases.

6. RELATED WORK

The most related works are [15, 28, 31]. In [15], a terrain map or 3D model of the environment is used to predict the channel. Unfortunately, such models are seldom available and, furthermore, their resolution is typically very low relative to typical wavelengths, which indicates that the resulting accuracy may be insufficient for placement purposes. Besides, a reinforcement learning approach is used rather than a convex optimization approach as in the present paper. The algorithm needs to be retrained in every new environment or if the number of UAVs changes. Besides, this approach is not flexible enough to accommodate additional constraints, for example that a human user must take control of one of the UAVs.

The approach in [31] relies on average local descriptors of the channel in terms of a map that provides the path loss exponent of each region in the deployment scenario. However, it just applies for $N = M = 1$.

Finally, [28] also adopts a convex optimization approach based on promoting sparsity, but the formulation is entirely different as it is not based on a discretization. Its complexity is $\mathcal{O}(M^6)$, which restricts its applicability to scenarios with a low number of GTs. Besides, it cannot accommodate general flight constraints since convexity would be lost in that case.

7. CONCLUSIONS

This paper proposes a new approach to ABS placement where, instead of relying on average characterizations of the channel, a radio map of the specific deployment scenario is constructed and used to determine the set of optimal ABS locations in terms of a convex objective that approximately minimizes the number of ABSs to guarantee a minimum rate to all GTs. Unlike most approaches, the proposed algorithm has a low complexity and can accommodate flight constraints such as no-fly zones or airspace occupied by buildings. The intuitive soundness of the scheme is empirically corroborated using an open source simulator developed in this work.

8. REFERENCES

[1] Y. Zeng, Q. Wu, and R. Zhang, "Accessing from the sky: A tutorial on UAV communications for 5G and beyond," *arXiv preprint arXiv:1903.05289*, 2019.

[2] Z. Han, A. L. Swindlehurst, and K. J. R. Liu, "Optimization of manet connectivity via smart deployment/movement of unmanned air vehicles," *IEEE Trans. Veh. Technol.*, vol. 58, no. 7, pp. 3533–3546, 2009.

[3] I. Bor-Yaliniz, A. El-Keyi, and H. Yanikomeroglu, "Efficient 3-d placement of an aerial base station in next generation cellular networks," in *Proc. IEEE Int. Conf. Commun.* IEEE, 2016, pp. 1–5.

[4] J. Chen and D. Gesbert, "Optimal positioning of flying relays for wireless networks: A LOS map approach," in *Proc. IEEE Int. Conf. Commun.*, Paris, France, May 2017, pp. 1–6.

[5] Z. Wang, L. Duan, and R. Zhang, "Adaptive deployment for UAV-aided communication networks," *IEEE Trans. Wireless Commun.*, vol. 18, no. 9, pp. 4531–4543, 2019.

[6] D. Romero and G. Leus, "Non-cooperative aerial base station placement via stochastic optimization," in *Proc. IEEE Mobile Ad-hoc Sensor Netw.*, Shenzhen, China, Dec. 2019, pp. 131–136.

[7] S. Park, K. Kim, H. Kim, and H. Kim, "Formation control algorithm of multi-uav-based network infrastructure," *Applied Sciences*, vol. 8, no. 10, pp. 1740, 2018.

[8] D.-Y. Kim and J.-W. Lee, "Integrated topology management in flying ad hoc networks: Topology construction and adjustment," *IEEE Access*, vol. 6, pp. 61196–61211, 2018.

[9] A. Al-Hourani, S. Kandeepan, and A. Jamalipour, "Modeling air-to-ground path loss for low altitude platforms in urban environments," in *IEEE Global Commun. Conf.*, 2014, pp. 2898–2904.

[10] E. Kalantari, H. Yanikomeroglu, and A. Yongacoglu, "On the number and 3D placement of drone base stations in wireless cellular networks," in *IEEE Vehicular Tech. Conf.*, 2016, pp. 1–6.

[11] H. El Hammouti, M. Benjillali, B. Shihada, and M.-S. Alouini, "A distributed mechanism for joint 3D placement and user association in UAV-assisted networks," in *IEEE Wireless Commun. Netw. Conf.*, Marrakech, Morocco, Apr. 2019.

[12] B. Perabathini, K. Tummuri, A. Agrawal, and V.S. Varma, "Efficient 3D placement of UAVs with QoS Assurance in Ad Hoc Wireless Networks," in *Int. Conf. Comput. Commun. Netw.*, 2019, pp. 1–6.

[13] X. Liu, Y. Liu, and Y. Chen, "Reinforcement learning in multiple-UAV networks: Deployment and movement design," *IEEE Trans. Veh. Tech.*, vol. 68, no. 8, pp. 8036–8049, 2019.

[14] M.K. Shehzad, A. Ahmad, S.A. Hassan, and H. Jung, "Backhaul-aware intelligent positioning of UAVs and association of terrestrial base stations for fronthaul connectivity," *IEEE Trans. Netw. Sci. Eng.*, pp. 1–1, 2021.

[15] J. Qiu, J. Lyu, and L. Fu, "Placement optimization of aerial base stations with deep reinforcement learning," in *IEEE Int. Conf. Commun.*, 2020, pp. 1–6.

[16] J. Sabzehali, V.K. Shah, H.S. Dhillon, and J.H. Reed, "3D placement and orientation of mmWave-based UAVs for Guaranteed LoS Coverage," *IEEE Wireless Commun. Letters*, pp. 1–1, 2021.

[17] N. Patwari and P. Agrawal, "Nesh: A joint shadowing model for links in a multi-hop network," in *Proc. IEEE Int. Conf. Acoust., Speech, Signal Process.*, Las Vegas, NV, Mar. 2008, pp. 2873–2876.

[18] N. Patwari and P. Agrawal, "Effects of correlated shadowing: Connectivity, localization, and RF tomography," in *Proc. Int. Conf. Info. Process. Sensor Networks*, St. Louis, MO, Apr. 2008, pp. 82–93.

[19] D. Romero, Pham Q. Viet, and G. Leus, "Aerial base station placement leveraging radio tomographic maps," in *arXiv:2109.07372*, 2021.

[20] D. Romero, D. Lee, and G. B. Giannakis, "Blind radio tomography," *IEEE Trans. Signal Process.*, vol. 66, no. 8, pp. 2055–2069, Jan. 2018.

[21] J. Wilson, N. Patwari, and O. G. Vasquez, "Regularization methods for radio tomographic imaging," in *Virginia Tech Symp. Wireless Personal Commun.*, Blacksburg, VA, Jun. 2009.

[22] M. A. Kanso and M. G. Rabbat, "Compressed rf tomography for wireless sensor networks: Centralized and decentralized approaches," in *Int. Conf. Distributed Comput. Sensor Syst.*, Marina del Rey, CA, 2009, Springer, pp. 173–186.

[23] B. R. Hamilton, X. Ma, R. J. Baxley, and S. M. Matechik, "Propagation modeling for radio frequency tomography in wireless networks," *IEEE J. Sel. Topics Signal Process.*, vol. 8, no. 1, pp. 55–65, Feb. 2014.

[24] J.R. Mitchell, P. Dickof, and A.G. Law, "A comparison of line integral algorithms," *Comput. Physics*, vol. 4, no. 2, pp. 166–172, 1990.

[25] T. Lin, S. Ma, Y. Ye, and S. Zhang, "An ADMM-based interior-point method for large-scale linear programming," *Optim. Methods Software*, vol. 36, no. 2-3, pp. 389–424, 2021.

[26] S. Boyd, N. Parikh, E. Chu, B. Peleato, and J. Eckstein, "Distributed optimization and statistical learning via the alternating direction method of multipliers," *Found. Trends Mach. Learn.*, vol. 3, no. 1, pp. 1–122, Jan. 2011.

[27] E.J. Candes, M.B. Wakin, and S.P. Boyd, "Enhancing sparsity by reweighted ℓ_1 minimization," *J. Fourier Analysis App.*, vol. 14, no. 5, pp. 877–905, 2008.

[28] M. Huang, L. Huang, S. Zhong, and P. Zhang, "UAV-mounted mobile base station placement via sparse recovery," *IEEE Access*, vol. 8, pp. 71775–71781, 2020.

[29] B. Galkin, J. Kibilda, and L.A. DaSilva, "Deployment of UAV-mounted access points according to spatial user locations in two-tier cellular networks," in *Wireless Days*. IEEE, 2016, pp. 1–6.

[30] J. Lyu, Y. Zeng, R. Zhang, and T.J. Lim, "Placement optimization of UAV-mounted mobile base stations," *IEEE Commun. Letters*, vol. 21, no. 3, pp. 604–607, 2017.

[31] J. Chen, U. Mitra, and D. Gesbert, "3D urban UAV relay placement: Linear complexity algorithm and analysis," *IEEE Trans. Wireless Commun.*, pp. 1–1, 2021.